Title

A Biocatalytic Platform for Synthesis of Chiral α-Trifluoromethylated Organoborons

Permalink

https://escholarship.org/uc/item/46p8g5b3

Journal

ACS Central Science, 5(2)

ISSN

2374-7943

Authors

Huang, Xiongyi
Garcia-Borràs, Marc
Miao, Kun
et al.

Publication Date

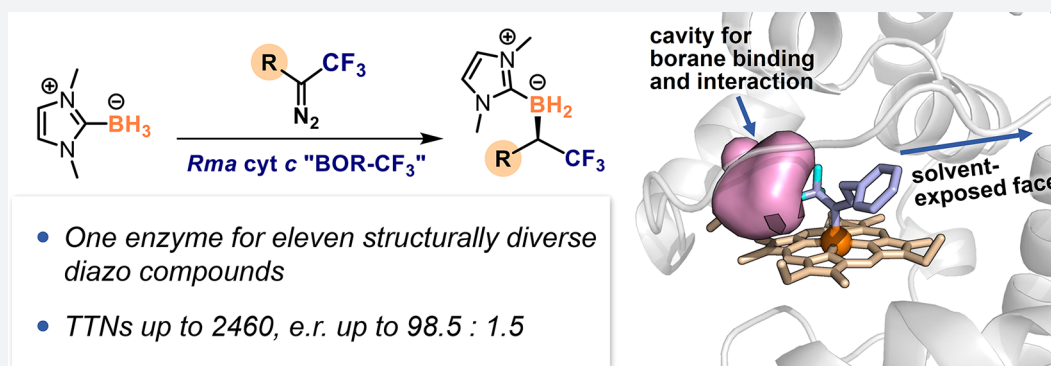2019-02-27

DOI

10.1021/acscentsci.8b00679

Peer reviewed

A Biocatalytic Platform for Synthesis of Chiral α-Trifluoromethylated Organoborons

Xiongyi Huang,[†,§] Marc Garcia-Borràs,[‡,§] Kun Miao,[†] S. B. Jennifer Kan,[†] Arjun Zutshi,[†] K. N. Houk,*[‡] and Frances H. Arnold*[†]

[†]Division of Chemistry and Chemical Engineering, California Institute of Technology, Pasadena, California 91125, United States
[‡]Department of Chemistry and Biochemistry, University of California, Los Angeles, California 90095, United States

Ⓢ *Supporting Information*

- *One enzyme for eleven structurally diverse diazo compounds*
- *TTNs up to 2460, e.r. up to 98.5 : 1.5*

ABSTRACT: There are few biocatalytic transformations that produce fluorine-containing molecules prevalent in modern pharmaceuticals. To expand the scope of biocatalysis for organofluorine synthesis, we have developed an enzymatic platform for highly enantioselective carbene B−H bond insertion to yield versatile α-trifluoromethylated (α-CF$_3$) organoborons, an important class of organofluorine molecules that contain stereogenic centers bearing both CF$_3$ and boron groups. In contrast to current "carbene transferase" enzymes that use a limited set of simple diazo compounds as carbene precursors, this system based on *Rhodothermus marinus* cytochrome *c* (*Rma* cyt *c*) can accept a broad range of trifluorodiazo alkanes and deliver versatile chiral α-CF$_3$ organoborons with total turnovers up to 2870 and enantiomeric ratios up to 98.5:1.5. Computational modeling reveals that this broad diazo scope is enabled by an active-site environment that directs the alkyl substituent on the heme CF$_3$-carbene intermediate toward the solvent-exposed face, thereby allowing the protein to accommodate diazo compounds with diverse structural features.

Fluorine-containing molecules have assumed a privileged position in modern medicine and comprise more than 20% of all pharmaceuticals.[1,2] Although many chemical methods for synthesis of organofluorines have been developed,[3,4] there is a noticeable lack of enzymatic approaches for their synthesis.[5] To expand the scope of biocatalytic fluorine chemistry, two main strategies are currently considered.[5,6] The first is to expand the substrate scope of natural fluorinase enzymes via protein engineering. The second is to modify biosynthetic pathways to accept fluorinated building blocks for precursor-directed biosynthesis. Although significant progress has been made,[5−13] both approaches suffer from restricted substrate scope and low efficiency, which hampers synthetic applications.

A promising strategy to expand the synthetic capability of nature is to introduce non-natural chemistries into existing proteins.[14−16] Enzymes that share similar mechanistic elements with non-natural reactions can exhibit promiscuous activities for abiological reactions, from which new activities can be evolved.[17,18] Here, we used this mechanism-driven approach to

develop fully genetically encoded enzymes that can perform non-natural reactions for organofluorine synthesis. Our target transformation is the synthesis of chiral α-trifluoromethylated (α-CF$_3$) organoborons from trifluorodiazo alkanes and Lewis-base borane complexes. This class of organofluorine compounds serves as valuable synthetic building blocks that can be converted to a broad range of CF$_3$-containing molecules via versatile boron-mediated transformations.[19−24] Despite the synthetic versatility of α-CF$_3$ organoborons, their asymmetric preparation remains a challenge. The few known enantioselective examples in synthetic chemistry include a copper-catalyzed asymmetric hydroboration of CF$_3$-substituted alkenes and enantioselective insertions of CF$_3$-carbene intermediates into B−H bonds of Lewis-base borane complexes.[21,25] The substrate scopes in both examples are very limited: the hydroboration approach has only been applied to aromatic β-CF$_3$-α,β-unsaturated ketones,[21] whereas
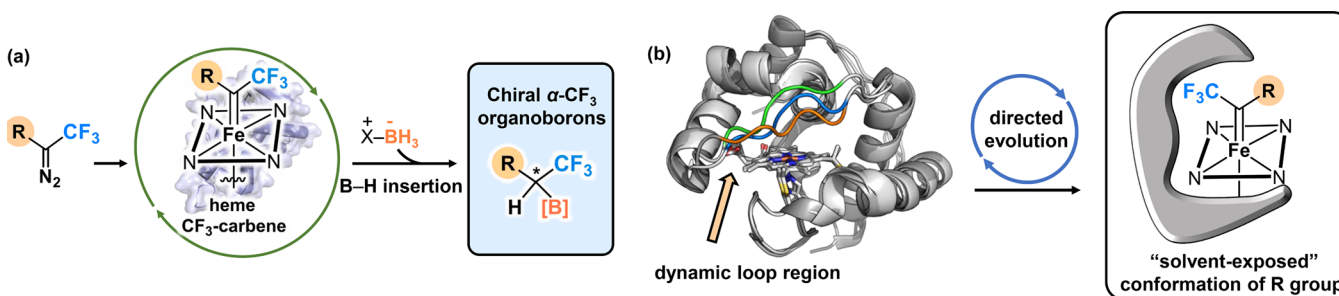
Figure 1. (a) Design of a general enzymatic platform for synthesis of chiral α-CF$_3$ organoborons. (b) On the left, overlay of *Rma* cyt *c* (PDB 3CP5, front loop region in blue), *Rma* TDE (PDB 6CUK, front loop region in orange), and *Rma* TDE with iron porphyrin carbene structure obtained from computational modeling (ref 52, front loop region in green). The large change in front loop structure highlights the impact loop mutations have on access to the active site of *Rma* cyt *c*. On the right, we propose that the active-site environment can be tuned to orient the heme-carbene intermediate such that the alkyl substituent R is solvent-exposed.
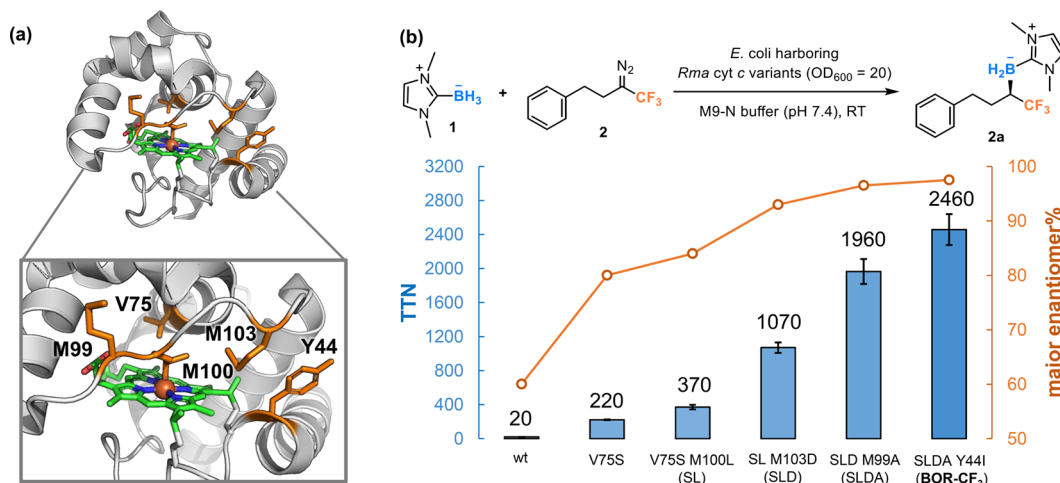

Figure 2. (a) X-ray crystal structure of wild-type *Rma* cyt *c* (PDB 3CP5). Residues targeted for site-saturation mutagenesis (V75, M99, M100, M103, and Y44) are shown in sticks. (b) Directed evolution of *Rma* cyt *c* for enantioselective synthesis of α-CF$_3$ organoborons with NHC borane **1** and diazo compound **2** as the model substrates. Reactions were performed in M9-N (pH 7.4) suspensions of *Escherichia coli* cells expressing *Rma* cyt *c* variants (OD$_{600}$ = 20). Standard reaction conditions were 10 mM borane substrate **1**, 7.5 mM diazo substrate **2**, room temperature under anaerobic conditions. Total turnovers (TTN) were defined as the amount of α-CF$_3$ organoboron product divided by the total amount of expressed *Rma* cyt *c* protein as determined by the hemochrome assay. The absolute configuration of product **2a** was determined to be *R* based on the optical rotation of the derivatized alcohol. See the Supporting Information, section VII, for detailed experimental procedures. wt refers to wild-type *Rma* cyt *c*. Single-letter abbreviations for the amino acid residues: V, Val; S, Ser; M, Met; L, Leu; D, Asp; A, Ala; Y, Tyr; I, Ile.

the B−H insertion strategy has only been demonstrated with a few aryl-substituted trifluorodiazo compounds.[25]

The deficit of methods for making chiral α-CF$_3$ organoborons motivated us to develop an enzymatic platform for their synthesis by reprogramming heme proteins to utilize trifluorodiazo alkanes for enantioselective carbene B−H bond insertion reactions (Figure 1a). Harnessing the facile synthetic accessibility of trifluorodiazo alkanes[26] and the evolvability of heme proteins,[16,27] this platform can be used to prepare a broad range of chiral α-CF$_3$ organoborons, many of which are currently unobtainable. The major challenge to developing the enzymatic system is engineering the heme proteins to accommodate structurally diverse heme CF$_3$-carbene intermediates for enantioselective B−H bond insertion. Although current carbene transferases can use a variety of substrates for versatile chemical transformations,[28−43] the scope of diazo compounds in most of these reactions has been very limited (mainly to ethyl diazoacetate (EDA)). To expand the diazo substrate scope, it has usually been necessary to reoptimize the enzyme active site for each new diazo substrate. Furthermore, for all synthetic carbene B−H bond insertion reactions

developed to date,[44−50] high enantioselectivity has only been achieved for diazo compounds containing (hetero)aromatic groups adjacent to the diazo carbon.

We envisioned that these challenges could be met by leveraging the unique structural features of *Rhodothermus marinus* cytochrome *c* (*Rma* cyt *c*).[51] This protein has proven to be a highly versatile platform for developing new enzymatic carbene-transfer reactions.[33,34] The heme-binding pocket of wild-type *Rma* cyt *c* is surrounded by several α-helices, two of which are connected by a surface loop.[51] Recent structural characterization of the laboratory-evolved *Rma* cyt *c* TDE carbene transferase with a bound iron porphyrin carbene (IPC) intermediate revealed that the three mutations introduced during directed evolution rendered this surface loop (residues 98−103) highly flexible (Figure 1b, left).[52] This enhanced flexibility allows the loop to explore more open conformations, not observed in the wild-type structure, that promote interactions between the substrate and the carbene intermediate. We hypothesized that we could engineer an active-site environment that favors a constrained conformation in which the CF$_3$ group of heme CF$_3$-carbene intermediates
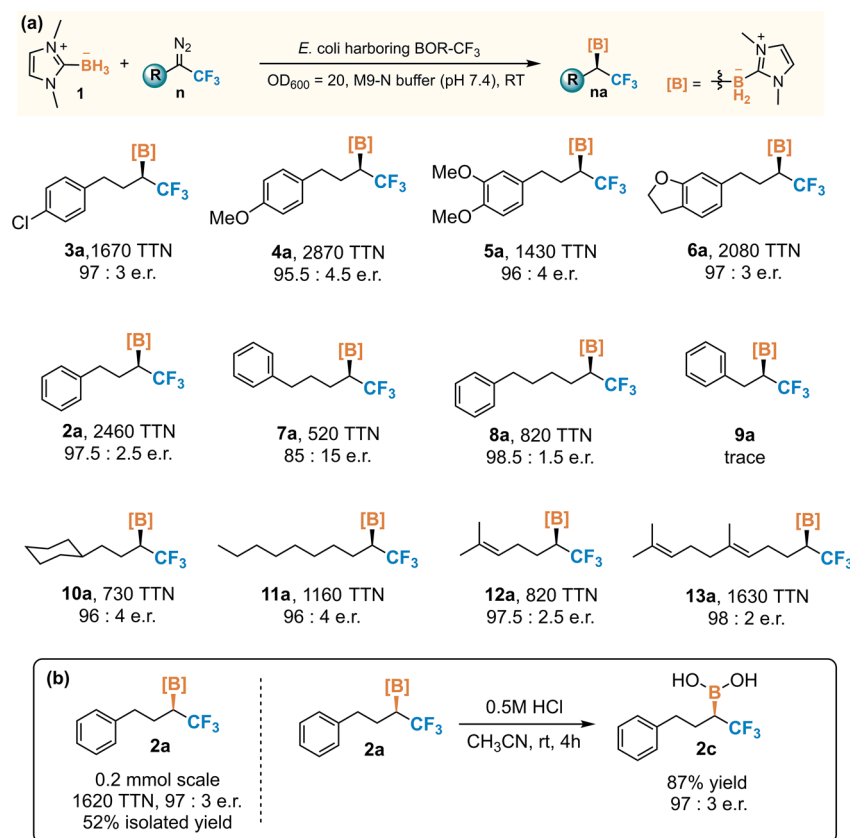
Figure 3. (a) Scope of trifluorodiazo alkanes for carbene B−H insertion catalyzed by BOR-CF$_3$. Reactions were performed in M9-N (pH 7.4) suspensions of *E. coli* cells expressing BOR-CF$_3$ (OD$_{600}$ = 20). Standard reaction conditions were 10 mM borane substrate **1**, 7.5 mM diazo substrate **n**, room temperature under anaerobic conditions. The absolute configuration of **2a** was determined to be *R* based on the optical rotation of the derivatized alcohol (see the Supporting Information, section VII). (b) Preparative scale synthesis (0.2 mmol scale) and the derivatization of **2a** to boronic acid **2c**.

points into the heme pocket, and the bulkier alkyl substituent R faces the solvent-exposed side (Figure 1b, right). In this conformation, the restricted orientation of the CF$_3$ group could ensure highly enantioselective formation of C−B bonds with little or no interference from the alkyl substituent R.

To identify mutations that can stabilize the conformation proposed in Figure 1b, we began directed evolution of *Rma* cyt *c* with *N*-heterocyclic carbene (NHC) borane **1** as the model borane substrate and (3-diazo-4,4,4-trifluorobutyl)benzene (**2** in Figure 2) as the model diazo carbene precursor. We expected that the large phenylethyl group in **2** would facilitate its positioning toward the solvent-exposed face. While wild-type *Rma* cyt *c* barely catalyzed carbene B−H insertion with **2**, site-saturation mutagenesis (SSM) at residue V75 led to the discovery of the V75S variant, which afforded the desired product **2a** with 220 total turnovers (TTN) and 80:20 enantiomeric ratio (e.r.). Residue V75 is located on an α-helix that is close to the heme cofactor and was previously shown to be a key site for expanding the scope of diazo compounds.[33] With *Rma* cyt *c* V75S as the parent, we performed additional rounds of SSM on residues M100, M103, T101, and M99 to further improve the catalytic performance of this borylation catalyst. These residues reside on the front loop and are important for controlling the structure of the heme pocket.[52] Through this engineering, we obtained a quadruple mutant, *Rma* cyt *c* V75S M100L M103D M99A (SLDA), which produced product **2a** with 1960 TTN and 96.5:3.5 e.r.

Y44 on the A helix of *Rma* cyt *c* is another residue that might affect catalysis of the target borylation reaction. In an *Rma* cyt *c*-catalyzed carbene Si−H insertion reaction, this residue was expected to interact with a silane substrate approaching the enzyme active site, as indicated by the crystal structure of an *Rma* cyt *c*-bound heme-carbene intermediate.[52] SSM of the quadruple mutant SLDA at Y44 and screening yielded the Y44I mutation that further improved borylation activity to 2460 TTN and enantioselectivity to 97.5:2.5 e.r.

With optimized variant *Rma* cyt *c* Y44I V75S M99A M100L M103D (denoted BOR-CF$_3$) in hand, we next probed its activity toward a panel of structurally diverse trifluorodiazo alkanes. If BOR-CF$_3$ stabilizes the "solvent-exposed" conformation of the R group as we expect, then it should accept a wide range of trifluorodiazo alkanes for enantioselective carbene B−H insertion. Indeed, as shown in Figure 3a, BOR-CF$_3$ could be used to synthesize a spectrum of α-CF$_3$ organoborons with diverse structural features. High enantioselectivity and activity were obtained for diazo compounds bearing different phenyl substitution patterns (**3a**−**6a**). Extending the chain length of the alkyl substituent R has a more profound impact on the performance of BOR-CF$_3$ (**7a**, **8a**). Strikingly, reducing the chain length to one carbon in **9a** abolishes borylation activity. As indicated by computational modeling, the iron-carbene intermediate generated from diazo **9** with a shorter alkyl chain can adopt conformations in which the phenyl moiety is close to the carbene reaction center. Unfavorable steric interactions with the phenyl group in these
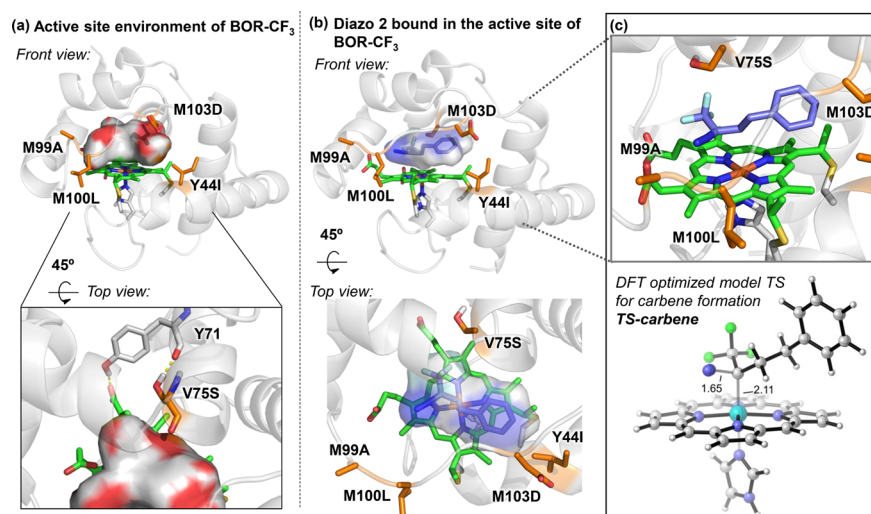
Figure 4. (a) The hydrogen bonding interactions between 75S and 71Y amide backbone and the empty surface area in a representative snapshot obtained from MD trajectories of BOR-CF$_3$ in the absence of diazo compound (see also Figures S1 and S2 in the Supporting Information). (b) Binding pose of diazo substrate **2** bound into the active site of BOR-CF$_3$, obtained from docking and constrained MD simulations (see Figure S3 and computational details in the SI). Direct comparison between the shape of the BOR-CF$_3$ active site and the docked diazo **2** shows the high complementarity achieved by evolution and introduction of V75S mutation. (c) Comparison of diazo **2** bound in the BOR-CF$_3$ structure and the DFT-optimized model transition state (TS) geometry for formation of the iron porphyrin carbene (IPC) intermediate (see the SI, Figure S8). The diazo **2** in this binding pose represents a near attack conformation that leads to the transition state for the generation of the iron porphyrin carbene intermediate.
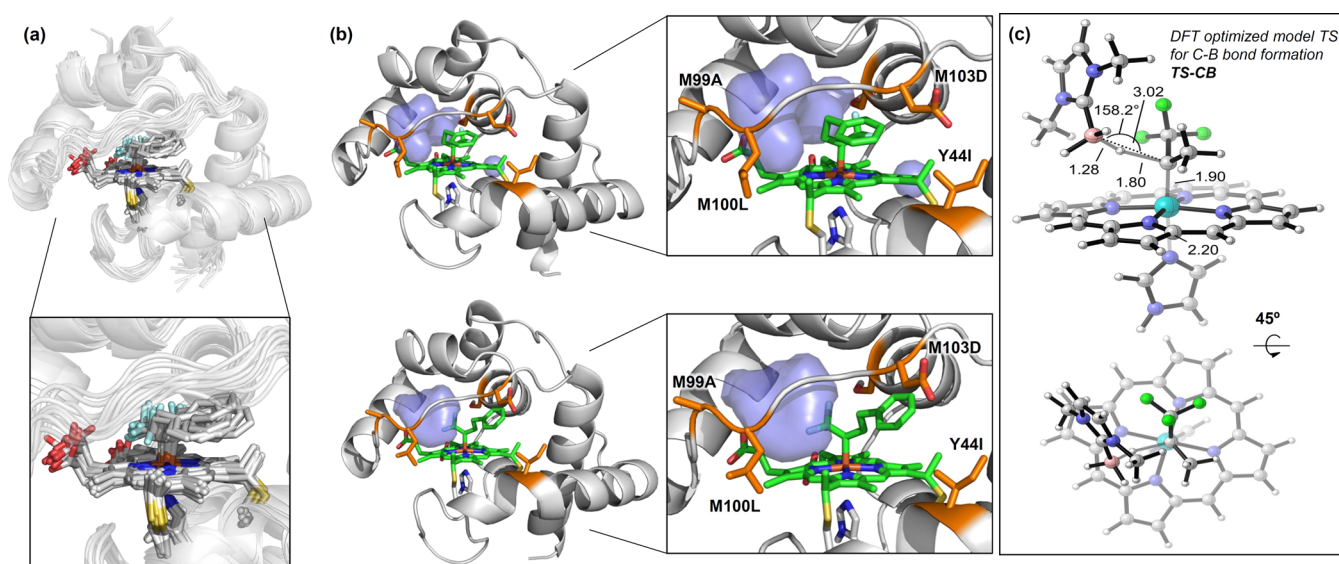

Figure 5. (a) Overlay of snapshots extracted from a 500 ns MD trajectory of BOR-CF$_3$-bound trifluoroalkyl-carbene intermediate **2b** (see also Figures S4 and S5 in the Supporting Information). (b) Representative snapshots of the two main conformations explored by trifluoroalkyl-carbene intermediate **2b** in BOR-CF$_3$ during MD trajectories. Blue surface represents the inner void cavity generated in the protein active site next to the iron porphyrin carbene. (c) DFT-optimized transition state (TS) for B–H carbene insertion in a model system (see also Figure S7). Key distances and angles are given in Å and degrees.

conformations would inhibit the borane substrate's approach to the carbene (see Figure S6 in the Supporting Information).

We further challenged BOR-CF$_3$ with trifluorodiazo alkanes containing alkyl chains without aromatic groups (**10−13**). Although these diazo compounds are structurally distinct from the model compound **2** used for directed evolution, BOR-CF$_3$ can still effectively convert them into α-CF$_3$ organoborons with 730−1630 TTN and 96:4−98:2 e.r. (**10a−13a**). This result shows that the high enantioselectivity of BOR-CF$_3$ does not require specific recognition of the aromatic substituent. One synthetic advantage of this method is that the trifluorodiazo

alkane starting compounds can be synthesized easily from a variety of starting materials such as alkyl halides, aldehydes, and carboxylic acids.[26,53,54] As these compounds are widely present in nature, this method could provide a facile way to obtain chiral organoborons that contain motifs of complex natural products. To demonstrate this, we synthesized trifluorodiazo compound **13** bearing a geranyl structural motif. Subjecting **13** to the standard conditions described in Figure 3 with BOR-CF$_3$ as the catalyst afforded organoboron product **13a** with 1630 TTN and 98:2 e.r. Given the prevalence of the geranyl structural motif in bioactive

molecules,[55] this organoboron compound may find applications in syntheses of fluorinated analogues of natural products such as pheromones. To further demonstrate the synthetic utility of our method, we performed this biocatalytic transformation on preparative scale and obtained borane product **2a** in 52% isolated yield and 97:3 e.r. The NHC borane **2a** can be readily converted to the boronic acid **2c** while retaining the stereochemistry of the boron-substituted chiral center, which would facilitate its further derivatization to other chiral trifluoromethyl-containing molecules.

We next used molecular dynamics (MD) simulations to obtain further insights into the stereocontrol imposed by the enzyme and the roles of the introduced mutations. Analysis of the active-site shape of BOR-CF$_3$ in the absence of both substrates revealed that the hydroxyl group in the 75S side chain forms a hydrogen bond with the Y71 amide backbone, which directs the C$_\beta$ hydrogen of serine to face toward the heme (Figure 4a). Modeling of the active-site structure of BOR-CF$_3$ with a bound diazo compound **2** showed that this serine arrangement generates more space at the heme distal side to better accommodate the CF$_3$ group. As a result, diazo compound **2** can mainly be docked in one specific conformation in the BOR-CF$_3$ active site (Figure 4b). Intriguingly, this conformation is structurally analogous to the transition state for iron-carbene generation via N$_2$ loss (Figure 4c). This result suggests that the active-site environment of BOR-CF$_3$ not only constrains the conformation of the trifluorodiazo alkane, but also promotes the formation of the iron-carbene intermediate by facilitating the interaction between the diazo compound and the heme iron center.

We further modeled the BOR-CF$_3$-bound trifluoroalkyl-carbene intermediate **2b** formed from diazo compound **2**. MD simulations revealed that **2b** can adopt two major conformations as shown in Figure 5a,b. The main difference between the two conformers is the slight rotation of the Fe−C bond, which is possible because no specific contacts between the CF$_3$ group and the protein stabilize one conformation over the other. Nonetheless, in both conformations, the CF$_3$ group is pointing into the active site, and the bulkier phenyl group lies between the M103D and Y44I side chains and is exposed to the solvent, in line with our original hypothesis. More interestingly, both conformers of **2b** expose the same pro-*R* face of the carbene intermediate to the empty volume generated in the active site, consistent with the observed *R* absolute configuration of product **2a**. To better understand the interaction between the borane substrate **1** and the carbene intermediate **2b**, we used DFT calculations to describe the transition state (TS) for B−H carbene insertion using a model iron porphyrin system (see the SI, section VIII, for computational details). A structural comparison between this TS geometry and the structure of protein-bound carbene intermediate **2b** revealed that borane **1** can be effectively accommodated in the empty volume of **2b** where it can adopt a catalytically competent pose to reach the TS for C−B bond formation (**TS-CB**). In this reaction scheme, the newly introduced M99A and M100L mutations alter the conformational dynamics of the front loop and generate an appropriate binding pocket for borane substrate **1** in the carbene-bound enzyme, while the major role of M103D and Y44I is to facilitate binding of the diazo substrate and stabilize both the diazo and the carbene intermediate in this binding pose. Notably, in this interaction mode, the alkyl substituent R on the CF$_3$-carbene intermediate should have little influence on

how the borane substrate approaches the carbene intermediate, which explains the general high enantioselectivity exhibited by BOR-CF$_3$ for most trifluorodiazo alkanes tested. The generality of this rationale for other trifluorodiazo alkanes is suggested by the catalytic performance of BOR-CF$_3$ and its earlier variants on geranyl-containing diazo compound **13**, where the trend in activity and enantioselectivity was similar to that with model diazo compound **2** (Scheme S1 in the Supporting Information).

In conclusion, we have developed a biocatalytic platform for synthesis of chiral α-CF$_3$ organoborons. Using directed evolution, we created an active site in *Rma* cyt *c* that can host structurally diverse trifluorodiazo alkanes for highly enantioselective carbene B−H insertion reactions. The effects of beneficial mutations on the catalytic activities and conformational dynamics have been rationalized by computational modeling. These efforts have expanded the scope of carbene intermediates accessible to heme proteins and provided new mechanistic insights into enzymatic carbene-transfer reactions.

■ ASSOCIATED CONTENT

ⓢ Supporting Information

The Supporting Information is available free of charge on the ACS Publications website at DOI: 10.1021/acscentsci.8b00679.

> Detailed experimental procedures, spectroscopic data for all new compounds, details for molecular dynamics (MD) simulations, and DFT calculations (PDF)

■ AUTHOR INFORMATION

Corresponding Authors

*E-mail: houk@chem.ucla.edu.
*E-mail: frances@cheme.caltech.edu.

ORCID ⓘ

Xiongyi Huang: 0000-0001-7156-8881
Marc Garcia-Borràs: 0000-0001-9458-1114
Kun Miao: 0000-0001-6567-3650
S. B. Jennifer Kan: 0000-0001-6371-8042
K. N. Houk: 0000-0002-8387-5261
Frances H. Arnold: 0000-0002-4027-364X

Author Contributions

§X.H. and M.G.-B. contributed equally to this work

Notes

The authors declare no competing financial interest.

■ ACKNOWLEDGMENTS

■ REFERENCES

(1) Purser, S.; Moore, P. R.; Swallow, S.; Gouverneur, V. Fluorine in medicinal chemistry. *Chem. Soc. Rev.* **2008**, *37*, 320−330.

(2) Meanwell, N. A. Fluorine and fluorinated motifs in the design and application of bioisosteres for drug design. *J. Med. Chem.* **2018**, *61*, 5822−5880.

(3) Liang, T.; Neumann, C. N.; Ritter, T. Introduction of fluorine and fluorine-containing functional groups. *Angew. Chem., Int. Ed.* **2013**, *52*, 8214−8264.

(4) Yang, X. Y.; Wu, T.; Phipps, R. J.; Toste, F. D. Advances in catalytic enantioselective fluorination, mono-, di-, and trifluoromethylation, and trifluoromethylthiolation reactions. *Chem. Rev.* **2015**, *115*, 826−870.

(5) Walker, M. C.; Chang, M. C. Y. Natural and engineered biosynthesis of fluorinated natural products. *Chem. Soc. Rev.* **2014**, *43*, 6527−6536.

(6) O'Hagan, D.; Deng, H. Enzymatic fluorination and biotechnological developments of the fluorinase. *Chem. Rev.* **2015**, *115*, 634−649.

(7) Thuronyi, B. W.; Chang, M. C. Y. Synthetic biology approaches to fluorinated polyketides. *Acc. Chem. Res.* **2015**, *48*, 584−592.

(8) Thuronyi, B. W.; Privalsky, T. M.; Chang, M. C. Y. Engineered fluorine metabolism and fluoropolymer production in living cells. *Angew. Chem., Int. Ed.* **2017**, *56*, 13637−13640.

(9) Thompson, S.; Zhang, Q.; Onega, M.; McMahon, S.; Fleming, I.; Ashworth, S.; Naismith, J. H.; Passchier, J.; O'Hagan, D. A localized tolerance in the substrate specificity of the fluorinase enzyme enables "last-step" ^{18}F fluorination of a RGD peptide under ambient aqueous conditions. *Angew. Chem., Int. Ed.* **2014**, *53*, 8913−8918.

(10) Eustaquio, A. S.; O'Hagan, D.; Moore, B. S. Engineering fluorometabolite production: fluorinase expression in *Salinispora tropica* yields fluorosalinosporamide. *J. Nat. Prod.* **2010**, *73*, 378−382.

(11) Walker, M. C.; Thuronyi, B. W.; Charkoudian, L. K.; Lowry, B.; Khosla, C.; Chang, M. C. Y. Expanding the fluorine chemistry of living systems using engineered polyketide synthase pathways. *Science* **2013**, *341*, 1089−1094.

(12) Weeks, A. M.; Wang, N.; Pelton, J. G.; Chang, M. C. Y. Entropy drives selective fluorine recognition in the fluoroacetyl-CoA thioesterase from *Streptomyces cattleya*. *Proc. Natl. Acad. Sci. U. S. A.* **2018**, *115*, E2193−E2201.

(13) McMurry, J. L.; Chang, M. C. Y. Fluorothreonyl-tRNA deacylase prevents mistranslation in the organofluorine producer *Streptomyces cattleya*. *Proc. Natl. Acad. Sci. U. S. A.* **2017**, *114*, 11920−11925.

(14) Arnold, F. H. Directed evolution: bringing new chemistry to life. *Angew. Chem., Int. Ed.* **2018**, *57*, 4143−4148.

(15) Prier, C. K.; Arnold, F. H. Chemomimetic biocatalysis: Exploiting the synthetic potential of cofactor-dependent enzymes to create new catalysts. *J. Am. Chem. Soc.* **2015**, *137*, 13992−14006.

(16) Brandenberg, O. F.; Fasan, R.; Arnold, F. H. Exploiting and engineering hemoproteins for abiological carbene and nitrene transfer reactions. *Curr. Opin. Biotechnol.* **2017**, *47*, 102−111.

(17) Khersonsky, O.; Tawfik, D. S. Enzyme promiscuity: A mechanistic and evolutionary perspective. *Annu. Rev. Biochem.* **2010**, *79*, 471−505.

(18) Khersonsky, O.; Roodveldt, C.; Tawfik, D. S. Enzyme promiscuity: Evolutionary and mechanistic aspects. *Curr. Opin. Chem. Biol.* **2006**, *10*, 498−508.

(19) Molander, G. A.; Ryu, D. Diastereoselective synthesis of vicinally bis(trifluoromethylated) alkylboron compounds through successive insertions of 2,2,2-trifluorodiazoethane. *Angew. Chem., Int. Ed.* **2014**, *53*, 14181−14185.

(20) Argintaru, O. A.; Ryu, D.; Aron, I.; Molander, G. A. Synthesis and applications of α-trifluoromethylated alkylboron compounds. *Angew. Chem., Int. Ed.* **2013**, *52*, 13656−13660.

(21) Jiang, Q.; Guo, T.; Yu, Z. Copper-catalyzed asymmetric borylation: construction of a stereogenic carbon center bearing both CF$_3$ and organoboron functional groups. *J. Org. Chem.* **2017**, *82*, 1951−1960.

(22) Fyfe, J. W. B.; Watson, A. J. B. Recent developments in organoboron chemistry: Old dogs, new tricks. *Chem.* **2017**, *3*, 31−55.

(23) Ryu, D.; Primer, D. N.; Tellis, J. C.; Molander, G. A. Single-electron transmetalation: synthesis of 1,1-diaryl-2,2,2-trifluoroethanes by photoredox/nickel dual catalytic cross-coupling. *Chem. - Eur. J.* **2016**, *22*, 120−123.

(24) Sandford, C.; Aggarwal, V. K. Stereospecific functionalizations and transformations of secondary and tertiary boronic esters. *Chem. Commun.* **2017**, *53*, 5481−5494.

(25) Hyde, S.; Veliks, J.; Liégault, B.; Grassi, D.; Taillefer, M.; Gouverneur, V. Copper-catalyzed insertion into heteroatom−hydrogen bonds with trifluorodiazoalkanes. *Angew. Chem., Int. Ed.* **2016**, *55*, 3785−3789.

(26) Shi, G.; Xu, Y. A facile synthesis of α-trifluorodiazo compounds. *J. Fluorine Chem.* **1990**, *46*, 173−178.

(27) Wang, J. B.; Li, G.; Reetz, M. T. Enzymatic site-selectivity enabled by structure-guided directed evolution. *Chem. Commun.* **2017**, *53*, 3916−3928.

(28) Brandenberg, O. F.; Prier, C. K.; Chen, K.; Knight, A. M.; Wu, Z.; Arnold, F. H. Stereoselective enzymatic synthesis of heteroatom-substituted cyclopropanes. *ACS Catal.* **2018**, *8*, 2629−2634.

(29) Hernandez, K. E.; Renata, H.; Lewis, R. D.; Kan, S. B. J.; Zhang, C.; Forte, J.; Rozzell, D.; McIntosh, J. A.; Arnold, F. H. Highly stereoselective biocatalytic synthesis of key cyclopropane intermediate to ticagrelor. *ACS Catal.* **2016**, *6*, 7810−7813.

(30) Knight, A. M.; Kan, S. B. J.; Lewis, R. D.; Brandenberg, O. F.; Chen, K.; Arnold, F. H. Diverse engineered heme proteins enable stereodivergent cyclopropanation of unactivated alkenes. *ACS Cent. Sci.* **2018**, *4*, 372−377.

(31) Coelho, P. S.; Wang, Z. J.; Ener, M. E.; Baril, S. A.; Kannan, A.; Arnold, F. H.; Brustad, E. M. A serine-substituted P450 catalyzes highly efficient carbene transfer to olefins *in vivo*. *Nat. Chem. Biol.* **2013**, *9*, 485−487.

(32) Coelho, P. S.; Brustad, E. M.; Kannan, A.; Arnold, F. H. Olefin cyclopropanation via carbene transfer catalyzed by engineered cytochrome P450 enzymes. *Science* **2013**, *339*, 307−310.

(33) Kan, S. B. J.; Huang, X.; Gumulya, Y.; Chen, K.; Arnold, F. H. Genetically programmed chiral organoborane synthesis. *Nature* **2017**, *552*, 132−136.

(34) Kan, S. B. J.; Lewis, R. D.; Chen, K.; Arnold, F. H. Directed evolution of cytochrome *c* for carbon−silicon bond formation: Bringing silicon to life. *Science* **2016**, *354*, 1048−1051.

(35) Yang, H.; Swartz, A. M.; Park, H. J.; Srivastava, P.; Ellis-Guardiola, K.; Upp, D. M.; Lee, G.; Belsare, K.; Gu, Y.; Zhang, C.; Moellering, R. E.; Lewis, J. C. Evolving artificial metalloenzymes via random mutagenesis. *Nat. Chem.* **2018**, *10*, 318−324.

(36) Srivastava, P.; Yang, H.; Ellis-Guardiola, K.; Lewis, J. C. Engineering a dirhodium artificial metalloenzyme for selective olefin cyclopropanation. *Nat. Commun.* **2015**, *6*, 7789.

(37) Bajaj, P.; Sreenilayam, G.; Tyagi, V.; Fasan, R. Gram-scale synthesis of chiral cyclopropane-containing drugs and drug precursors with engineered myoglobin catalysts featuring complementary stereoselectivity. *Angew. Chem., Int. Ed.* **2016**, *55*, 16110−16114.

(38) Bordeaux, M.; Tyagi, V.; Fasan, R. Highly Diastereoselective and Enantioselective Olefin Cyclopropanation Using Engineered Myoglobin-Based Catalysts. *Angew. Chem., Int. Ed.* **2015**, *54*, 1744−1748.

(39) Tyagi, V.; Fasan, R. Myoglobin-catalyzed olefination of aldehydes. *Angew. Chem., Int. Ed.* **2016**, *55*, 2512−2516.

(40) Sreenilayam, G.; Fasan, R. Myoglobin-catalyzed intermolecular carbene N-H insertion with arylamine substrates. *Chem. Commun.* **2015**, *51*, 1532−1534.

(41) Tinoco, A.; Steck, V.; Tyagi, V.; Fasan, R. Highly diastereo- and enantioselective synthesis of trifluoromethyl-substituted cyclopropanes via myoglobin-catalyzed transfer of trifluoromethylcarbene. *J. Am. Chem. Soc.* **2017**, *139*, 5293−5296.

(42) Dydio, P.; Key, H. M.; Nazarenko, A.; Rha, J. Y.-E.; Seyedkazemi, V.; Clark, D. S.; Hartwig, J. F. An artificial metal-

loenzyme with the kinetics of native enzymes. *Science* **2016**, *354*, 102−106.

(43) Key, H. M.; Dydio, P.; Clark, D. S.; Hartwig, J. F. Abiological catalysis by artificial haem proteins containing noble metals in place of iron. *Nature* **2016**, *534*, 534−537.

(44) Pang, Y.; He, Q.; Li, Z. Q.; Yang, J. M.; Yu, J. H.; Zhu, S. F.; Zhou, Q. L. Rhodium-Catalyzed B-H Bond Insertion Reactions of Unstabilized Diazo Compounds Generated in Situ from Tosylhydrazones. *J. Am. Chem. Soc.* **2018**, *140*, 10663−10668.

(45) Yang, J.-M.; Li, Z.-Q.; Li, M.-L.; He, Q.; Zhu, S.-F.; Zhou, Q.-L. Catalytic B−H bond insertion reactions using alkynes as carbene precursors. *J. Am. Chem. Soc.* **2017**, *139*, 3784−3789.

(46) Chen, D.; Zhang, X.; Qi, W.-Y.; Xu, B.; Xu, M.-H. Rhodium(I)-catalyzed asymmetric carbene insertion into B−H bonds: Highly enantioselective access to functionalized organoboranes. *J. Am. Chem. Soc.* **2015**, *137*, 5268−5271.

(47) Allen, T. H.; Kawamoto, T.; Gardner, S.; Geib, S. J.; Curran, D. P. *N*-Heterocyclic carbene boryl iodides catalyze insertion reactions of *N*-heterocyclic carbene boranes angoodd diazoesters. *Org. Lett.* **2017**, *19*, 3680−3683.

(48) Li, X.; Curran, D. P. Insertion of reactive rhodium carbenes into boron−hydrogen bonds of stable *N*-heterocyclic carbene boranes. *J. Am. Chem. Soc.* **2013**, *135*, 12076−12081.

(49) Cheng, Q.-Q.; Zhu, S.-F.; Zhang, Y.-Z.; Xie, X.-L.; Zhou, Q.-L. Copper-catalyzed B−H bond insertion reaction: a highly efficient and enantioselective C−B bond-forming reaction with amine−borane and phosphine−borane adducts. *J. Am. Chem. Soc.* **2013**, *135*, 14094−14097.

(50) Yang, J.-M.; Zhao, Y.-T.; Li, Z.-Q.; Gu, X.-S.; Zhu, S.-F.; Zhou, Q.-L. Gold-catalyzed oxidative coupling of terminal alkynes and borane adducts: efficient synthesis of *α*-boryl ketones. *ACS Catal.* **2018**, *8*, 7351−7355.

(51) Stelter, M.; Melo, A. M. P.; Pereira, M. M.; Gomes, C. M.; Hreggvidsson, G. O.; Hjorleifsdottir, S.; Saraiva, L. M.; Teixeira, M.; Archer, M. A novel type of monoheme cytochrome *c*: biochemical and structural characterization at 1.23 Å resolution of *Rhodothermus marinus* cytochrome *c*. *Biochemistry* **2008**, *47*, 11953−11963.

(52) Lewis, R. D.; Garcia-Borràs, M.; Chalkley, M. J.; Buller, A. R.; Houk, K. N.; Kan, S. B. J.; Arnold, F. H. Catalytic iron-carbene intermediate revealed in a cytochrome *c* carbene transferase. *Proc. Natl. Acad. Sci. U. S. A.* **2018**, *115*, 7308−7313.

(53) Wiedemann, J.; Heiner, T.; Mloston, G.; Prakash, G. K. S.; Olah, G. A. Direct preparation of trifluoromethyl ketones from carboxylic esters: trifluoromethylation with (trifluoromethyl)-trimethylsilane. *Angew. Chem., Int. Ed.* **1998**, *37*, 820−821.

(54) Bégué, J.-P.; Bonnet-Delpon, D. Preparation of trifluoromethyl ketones and related fluorinated ketones. *Tetrahedron* **1991**, *47*, 3207−3258.

(55) Matsuda, Y.; Abe, I. Biosynthesis of fungal meroterpenoids. *Nat. Prod. Rep.* **2016**, *33*, 26−53.